Physics Letters A 373 (2009) 3459–3463

Contents lists available at ScienceDirect

Physics Letters A

www.elsevier.com/locate/pla

Determination of preferential rare earth adatom adsorption geometries on Si(001)

Aniketa Shinde [a,b], Juexian Cao [a], Wenjie Ouyang [a], Ruqian Wu [a], Regina Ragan [b,*]

[a] Department of Physics & Astronomy, 4129 Frederick Reines Hall, University of California Irvine, Irvine, CA 92697-4575, USA
[b] Department of Chemical Engineering & Materials Science, 916 Engineering Tower, University of California Irvine, Irvine, CA 92697-2575, USA

ARTICLE INFO

Article history:
Received 8 July 2009
Received in revised form 22 July 2009
Accepted 23 July 2009
Available online 29 July 2009
Communicated by V.M. Agranovich

Keywords:
Scanning probe microscopy
Ab initio calculations
Rare earth disilicide
Self assembly
Formation energy

ABSTRACT

The adsorption patterns of rare earth atoms on Si(001) were investigated using scanning tunneling microscopy measurements and density functional calculations. Stable configurations were systematically determined via calculation of binding energies of various adatom coverage and adsorption geometry. Competition between inter-adatom hybridization and Coulomb repulsion is the mechanism contributing to binding energy minima associated with commonly observed rare earth adsorption geometries. Comparison of stable configurations with experimental scanning tunneling microscopy images demonstrated accuracy of the theoretical models. This paves a way for the understanding of self-assembly of rare earth disilicide nanowires on vicinal Si(001) substrates.

1. Introduction

Self-organization of rare earth adatoms at near monolayer coverage on Si(001) is known to result in formation of rare earth disilicide ($RESi_{2-x}$) metallic nanowires with high aspect ratios when annealed near 600 °C [1–4]. These nanowires have been of great interest due to their high conductivity and low Schottky barrier on *n*-type silicon [5–8], suitable for potential use as nanoscale interconnects [9]. Furthermore, uniform high-density $RESi_{2-x}$ nanowires have also demonstrated utility as templates for assembly of Au [10] and Pt [11] nanoclusters that may have interesting catalytic properties [12,13]. Yet understanding of the physical processes governing their growth, starting from the morphology of adsorption, is still not complete. This motivates us to perform systematic experimental and theoretical investigations for the coverage dependence of complex distribution patterns of rare earth adatoms on Si(001).

Since disilicide nanostructures are fabricated in ultra high vacuum (UHV), surface evolution during growth can be probed with atomic resolution. Scanning tunneling microscopy (STM) images can then be directly compared to results of density functional calculations, which provide deeper insight into nucleation mechanisms. We previously determined the four-fold hollow site as the energetically preferred binding site for an isolated RE adatom on Si(001) [14]; a result that was also found in an independent study [15]. Correct interpretation of STM images was enabled by construction of charge density above the surface according to the Tersoff–Hamann equation [16]. The formation of surface dipoles due to charge transfer from RE adatoms to Si(001) was predicted and experimentally confirmed by scanning Kelvin probe force microscopy measurements [17]. Due to charge depletion, RE adatoms are typically observed in empty states STM images [15,17,18].

In this Letter, we investigate stable adsorption patterns of RE on Si(001) at varying adatom coverage through systematic density functional calculations and STM measurements. To circumvent difficulties in dealing with strongly localized $4f$ electrons [19], we used yttrium to represent RE elements, a common practice in this context. Y is a trivalent atom that does not have f valence electrons but has chemical and physical properties very similar to RE atoms [20,21]. It was found that the atomic and electronic structures of YSi_2 monolayers on Si(111) resemble $RESi_{2-x}$ thin films very well [22,23]. Here we found that geometries associated with total energy minima correlate with experimentally observed (2×3) [3,24,25], (2×4) [14,18,19,26,27], and (2×7) [18,19,27,28] surface reconstructions. Clear understanding of adatom adsorption patterns is achieved through extensive analysis of electronic structures. Moreover, we discuss the influence of these adsorption geometries on the nucleation of parallel arrays of nanowires on vicinal Si(001) surfaces [2,3] as well as perpendicular nanowire arrays on nominally flat Si(001) [1,29]. This provides useful insights for future directed self-assembly strategies.

2. Methods

Experimentally, (2×1) reconstructed Si(001) surfaces were prepared by flashing at 1200 °C and rare earth deposition at

* Corresponding author. Tel.: +1 949 824 6830; fax: +1 949 824 2541.
E-mail address: rragan@uci.edu (R. Ragan).

0375-9601/$ – see front matter
doi:10.1016/j.physleta.2009.07.064

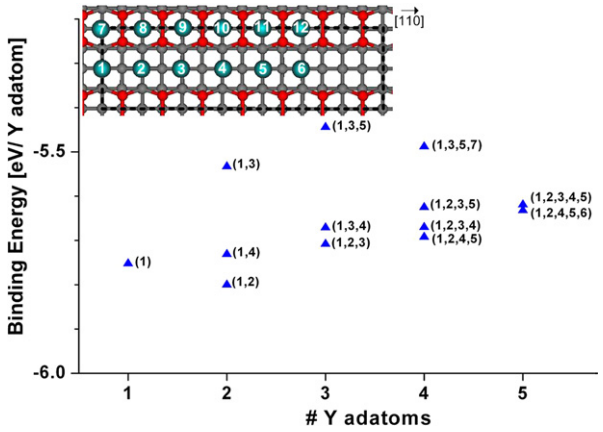

Fig. 1. (Color online.) Normalized binding energy plotted as a function of the number of Y adatoms and geometric configuration. The ball and stick figure in the upper left corner numbers possible adsorption sites for Y on Si(001) shown in cyan; Si surface dimers are colored red and bulk Si is gray. A black dashed rectangle outlines the (2×7) unit cell used in the binding energy calculations.

sub-monolayer coverage was performed at 600 °C in ultra high vacuum in accordance with methods published in our previous work [14]. Dysprosium, erbium or samarium was evaporated from a molybdenum crucible in an electron beam evaporator onto *p*-type Si(001) substrates. Samples were transferred to the analysis chamber without exposure to ambient conditions. Scanning tunneling microscopy imaging was performed at room temperature in ultra high vacuum [14,17].

First principles calculations were performed within the density-functional framework using the generalized gradient approximation (GGA) for the exchange correlation energy functional (PW 91), as implemented in the Vienna *ab initio* Simulation package (VASP) [30]. Ultra-soft pseudopotentials (US PP) were used to represent the electron interaction with ionic cores [31]. A plane-wave basis set with energy cutoff of 300 eV was used. We adopted a slab of 8 Si layers and a vacuum 15 Å thick to simulate the Si(001) substrate ($a_{Si} = 0.384$ nm). The bottom 3 layers of Si were fixed at their bulk positions and dangling bonds were passivated with hydrogen atoms. All other atoms were allowed to relax with a criterion that forces are lower than 0.01 eV/Å. Test calculations confirmed the adequacy of our model and parameters. Furthermore, the change in adsorption energy of a single Y adatom on a thicker 12 layer Si(001) slab was 11 meV, considerably lower than the thermal energy for RE deposition on Si at 600 °C ($k_bT = 75$ meV). In order to explore complex atomic configurations of Y adsorption, we used a (2×7) supercell in the lateral plane and $4 \times 1 \times 1$ *k*-points to sample the Bruillouin zone. Further test calculations for $6 \times 1 \times 1$ *k*-points showed that the binding energies converge to better than 20 meV.

3. Results and discussion

Using the (2×7) supercell, binding energy was calculated as a function of adatom coverage and adsorption geometry on the dimerized Si(001) surface [32]. The inset in the upper left of Fig. 1 shows the (2×7) supercell, with the energetically-preferred four-fold hollow binding sites [14] for Y denoted by cyan spheres. Note that sites 7–12 are not energetically preferred because of the condition that Si dimer bonds must first be broken [14]. In the following discussions, we characterize the stability of different adsorption geometries with a normalized binding energy (BE) defined as:

$$BE = (E_{Y/Si} - N^* E_Y - E_{Si})/N$$

where N is the number of Y adatoms, $E_{Y/Si}$ is the total energy of the system composed of N adatoms and the Si substrate, E_Y is the total energy of 1 Y atom in its bulk structure and E_{Si} is the total energy of the clean Si(001) 8 layer substrate. Interestingly, BE increases with adatom coverage (N), except for $N = 2$ where 2 adatoms are spaced 1 a_{Si} apart. Based on the results of the BE calculations, two physical mechanisms appear to affect BE. For an isolated adatom, we previously found significant charge transfer to the substrate, resulting in the experimental observation that RE adatoms carry a net positive charge [17,18]. Therefore, Coulomb repulsion tends to push Y adatoms apart. For instance, this leads to the decrease in BE for configuration $(1, 4)$ versus $(1, 3)$, since the $(1, 4)$ configuration has a larger Y–Y distance.

Inter-adatom hybridization is the competing mechanism to Coulomb repulsion that appears to play an important role since configuration $(1, 2)$ has a lower BE than an isolated Y adatom. The calculated Y–Y distance in this configuration is 3.88 Å [14] which is slightly larger than the Y–Y distance (3.84 Å) in bulk YSi_2 [32]. Evidence of Y adatom hybridization in the $(1, 2)$ configuration is demonstrated in the plots of charge density difference $[\Delta\rho = \rho(2Y/Si) - \rho(Si) - 2\rho(Y)]$ shown in Fig. 2. Figs. 2(a), (c) and (e) are top down views of charge density difference, while (b), (d) and (f) are cross sectional views for configurations $(1, 2)$, $(1, 3)$ and $(1, 4)$, respectively. Dark blue (green) contours represent areas with the greatest (smallest) charge depletion, while red (yellow) contours represent areas with the greatest (smallest) charge gain. The charge depletion from Y to adjacent surface Si atoms along the surface normal is evident in Figs. 2(a), (c) and (e) for configurations $(1, 2)$, $(1, 3)$ and $(1, 4)$, respectively, yet only Fig. 2(a) shows charge gain in the area between the two adatoms. Furthermore, in side view, Fig. 2(b) also shows significant charge accumulation between two Y adatoms, however this is not observed in the other configurations shown in (d) and (f). Because of the large separation between adatoms, no direct Y–Y hybridization is found for configurations $(1, 3)$ and $(1, 4)$, for which only charge transfer from Y to surface Si atoms is evident in Figs. 2(c)–(f). From Fig. 1, the continuous Y chain $(1, 2, 3)$ is still preferred for $N = 3$ but the BE is much higher than for $(1, 2)$. This is understandable since the Y adatoms at sites 1 and 3 experience Coulomb repulsion and only share electron density with the Y adatom at site 2. Configurations $(1, 3)$, $(1, 3, 5)$ and $(1, 3, 5, 7)$, with spacings of 2 a_{Si}, experience strong Coulomb repulsion but negligible Y–Y hybridization, and thus they have higher BE.

Our results explain why Y and RE tend to form chains with either 2 or 3 adatoms, as found in STM observations [15,19]. Clearly, this results from the competition between inter-adatom hybridization and long range Coulomb repulsion. Although the exact amount of charge transfer between neighboring RE adatoms might vary with the type of RE adatom and differ slightly from that of Y, the mechanisms discussed above should be generally applicable for all RE adatoms on Si(001). To demonstrate the validity of our calculations and applicability to RE/Si(001) systems, STM images were simulated for structures exhibiting BE minima and compared with experimental data. A relaxed ball and stick model of adatoms in configuration $(1, 2)$, which represents 2 Y adatoms spaced approximately 1 a_{Si} apart, is presented in Fig. 3(a) with the periodicity observed in the (2×3) surface reconstruction on a (4×3) Si(001) supercell. Cyan atoms are Y, red atoms are surface Si atoms and gray atoms represent subsurface Si. Si dimer rows are oriented along [110] and a dashed black rectangle highlights the (2×3) cell. An empty states STM simulation at $V_{bias} = +2.0$ V of this structure is shown in Fig. 3(b). The theoretical simulation for Y dimers correlates well with the experimental data. The observed (2×3) reconstruction resulting from Sm adatoms on Si(001) imaged with $V_{bias} = +2.0$ V and a feedback current of 100 pA is shown in Fig. 3(c) and matches well with the features displayed in Fig. 3(b). A white dashed box outlines the (2×3) cell and an oval highlights a region where adatoms form a row of Y perpendicular

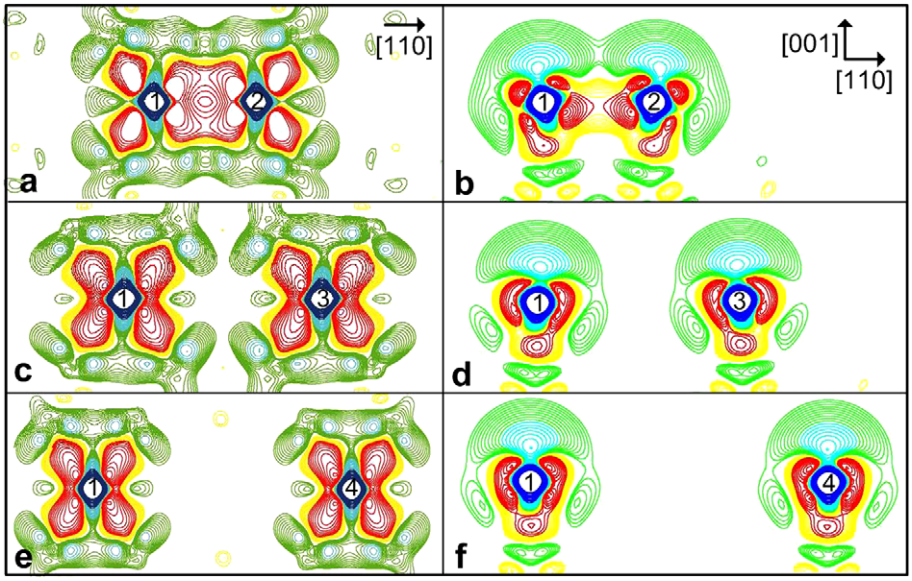

Fig. 2. (Color online.) Top down and side views of charge density difference for configurations (1, 2) in (a) and (b), (1, 3) in (c) and (d), and (1, 4) in (e) and (f), respectively. Contours begin from $+1 \times 10^{-5}$ $e/\text{Å}^3$ (green contours) and -1×10^{-5} $e/\text{Å}^3$ (yellow contours), representing charge loss and gain respectively, and change successively by a factor of 1.2. The greatest charge gain and depletion is represented by red and dark blue contours, respectively. The numbers represent the positions of Y adatoms as indicated by the inset in Fig. 1.

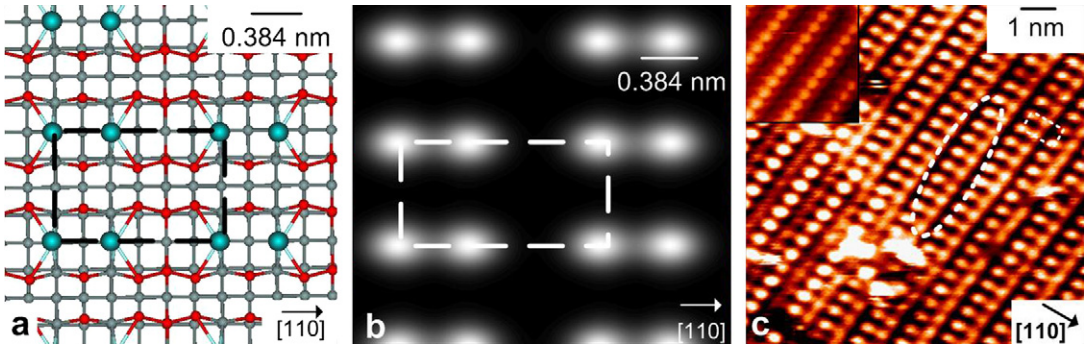

Fig. 3. (Color online.) (a) Relaxed ball and stick model represents atoms in the (1, 2) configuration with the (2×3) periodicity on a (4×3) Si(001) substrate. Y is represented slightly larger than Si in cyan; Si surface dimers are colored red and bulk Si is gray. (b) STM simulation of the structure on the left at $V_{\text{bias}} = +2.0$ V with the (2×3) unit cell outlined by a dashed white rectangle. (c) 10 nm × 10 nm STM image of Sm/Si(001) at $V_{\text{bias}} = +2.0$ V and feedback current of 140 pA. Dashed white oval outlines the Sm dimers that are oriented perpendicular to [110] and a dashed white rectangle outlines the (2×3) unit cell. The inset in (c) highlights the (2×3) reconstruction on the same sample at $V_{\text{bias}} = -1.0$ V.

to the original Si dimer rows. The simulation in Fig. 3(b) also correlates well with experimentally observed (2×3) reconstruction reported by others for Sm/Si(001) [3,24] and Er/Si(001) [25]. The inset in Fig. 3(c) shows the filled states image of Sm/Si(001) with $V_{\text{bias}} = -1.0$ V. It is interesting to note that the maximum intensity now shifts to the region in between adatoms rather than above Y adatom positions. The overlap in electron density between Sm adatom sites in filled states images further supports inter-adatom hybridization in RE adatoms as calculated for Y.

Configuration (1, 2, 3), corresponding to 3 Y adatoms each spaced approximately 1 a_{Si} apart, was found to have a BE minimum for 3 adatoms. A relaxed ball and stick schematic of configuration (1, 2, 3) with the periodicity observed in the (2×4) surface reconstruction is presented in Fig. 4(a) on a (4×4) Si(001) supercell. The STM simulation for configuration (1, 2, 3) is shown in Fig. 4(b) for imaging at $V_{\text{bias}} = +0.7$ V and the white dashed box indicates the (2×4) periodicity. This simulation is also in good agreement with the experimental data for Er/Si(001) displayed in Fig. 4(c), imaged at the same bias. Experimental STM images for Ho/Si(001) [27], Dy/Si(001) [26] and Gd/Si(001) [19] also have the same features. The white dashed oval at the bottom right corner of Fig. 4(c) highlights a region that has three protrusions making a chain along $[1\bar{1}0]$. Adatom locations correspond to the group of 3 intensity maxima with the center atom exhibiting the highest intensity. The intensity difference between central and edge Y is attributed to changes in local electronic structure on the surface rather than topography since relaxed structures did not show adatom buckling on the surface, as seen in the inset in Fig. 4(c).

The agreement between simulated structures with experimental STM images of Sm, Er and Dy presented here in addition to previous experimental STM results for Sm [3,24], Dy [26], Er [25], Ho [27], and Gd [28] supports the generality of the present models and discussions for different RE adatoms. Previous DFT calculations for Yb/Si(001) [15] assumed configurations of 2 and 3 adatoms spaced 1 a_{Si} apart on a bulk Si(001) surface and binding energies were compared for unique binding sites. In both cases, it was also found that the energetically preferred sites were four-fold hollow sites on Si(001) [14,15].

As RE coverage increases, adatoms create more complex patterns such as the well-known (2×7) reconstruction that has been observed for Dy [28], Gd [28] and Ho [18,27] on Si(001). The positions of electron density maxima in the (2×7) reconstruction have been discussed previously [19,28]; but no fully optimized atomic model was available. This surface reconstruction was at-

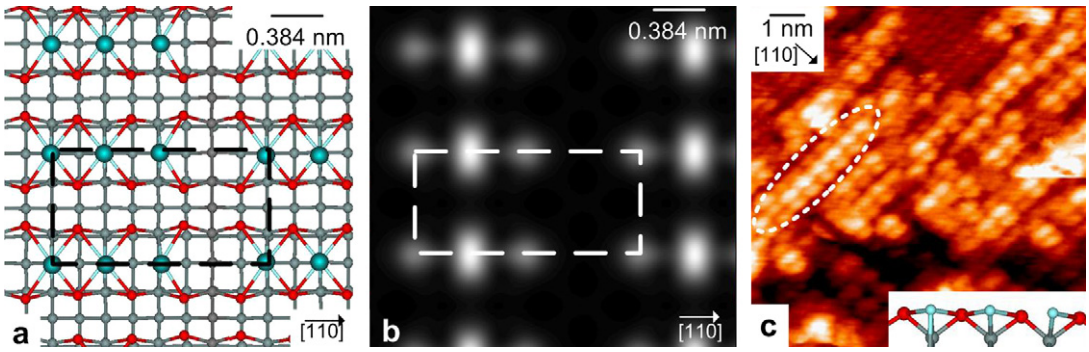

Fig. 4. (Color online.) (a) Relaxed ball and stick model of configuration (1, 2, 3) with the (2×4) periodicity on a (4×4) Si(001) substrate. Y is represented slightly larger than Si in cyan; Si surface dimers are colored red and bulk Si is gray. (b) Corresponding simulated STM image for $V_{\text{bias}} = +0.7$ V with a dashed white rectangle outlining the (2×4) unit cell. (c) 10 nm $\times$ 10 nm STM image of Er/Si(001) acquired with $V_{\text{bias}} = +0.7$ V and a feedback current of 100 pA showing groups of 3 maxima making a chain along [1$\bar{1}$0] as observed in the simulation in (b). The inset in (c) shows a cross section of the relaxed structure in (a) revealing the constant height of Y adatoms.

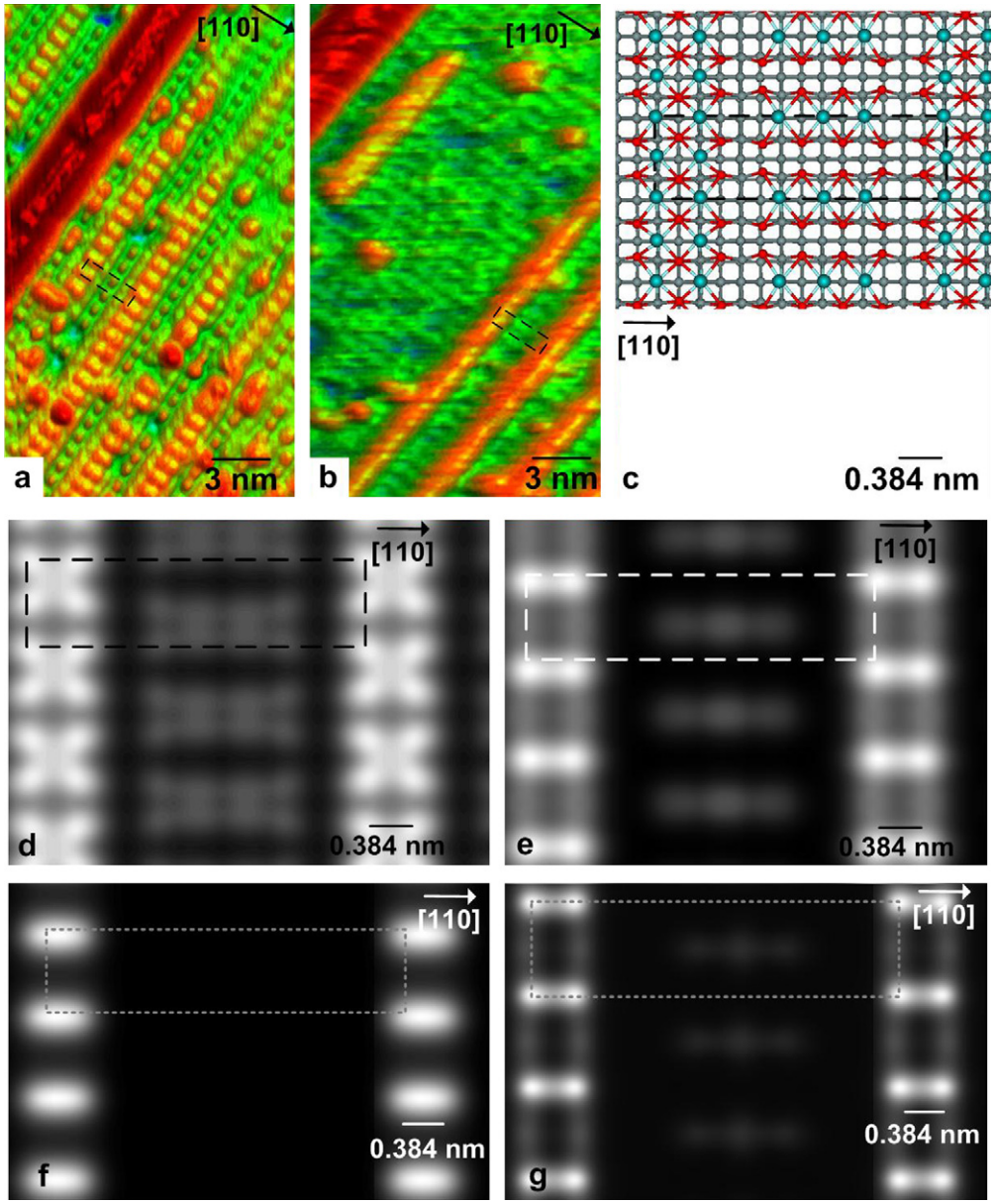

Fig. 5. (Color online.) STM images of Dy induced (2×7) reconstruction on Si(001) at (a) $V_{\text{bias}} = -1.9$ V and (b) $V_{\text{bias}} = +1.9$ V and feedback current of 100 pA. A dashed black rectangle outlines the (2×7) cell. (c) Relaxed ball and stick model for (2×7) reconstruction on a (2×7) Si(001) substrate. Y is represented slightly larger than Si in cyan; Si surface dimers are colored red and bulk Si is gray. Simulated STM images for (d) $V_{\text{bias}} = -1.9$ V, (e) $V_{\text{bias}} = +1.9$ V, (f) $V_{\text{bias}} = +0.28$ V and (g) $V_{\text{bias}} = +0.8$ V, with a dashed white rectangle outlining the (2×7) unit cell.

tributed to metal adatoms, not Si, on the surface, via metastable de-excitation spectroscopy of Ho on Si(001) [18]. If we examine the case of $N = 5$, configuration $(1, 2, 4, 5, 6)$ corresponds to the minimum BE, as seen in Fig. 1. This configuration combines $(1, 2)$ and $(1, 2, 3)$ and was previously assigned as the model for the (2×7) reconstruction by Harrison et al. Yet since full geometry optimization was not included in that work, adatoms were assumed to sit on different binding sites [19]. Furthermore, STM simulations for configuration $(1, 2, 4, 5, 6)$ do not completely emulate experimental STM observations. Figs. 5(a) and (b) are experimental filled and empty states STM images, respectively, for the Dy induced (2×7) reconstruction on Si(001). In empty states images, bright spots show the locations of RE adatoms, and a wire-like pattern is observed along $[1\bar{1}0]$ with a width of 2 a_{Si}. To establish a model that can reproduce this feature, adatoms need to be added at sites 7 and 8 to configuration $(1, 2, 4, 5, 6)$, as shown in Fig. 5(c). Indeed, sites 7–12 gradually become available with the presence of more Y adatoms since Si dimer atoms move apart by approximately 0.5 Å compared to the equilibrium dimer distance [33]. STM simulations of configuration $(1, 2, 4, 5, 6) + (7, 8)$ with the (2×7) periodicity at $V_{bias} = -1.9$ V and $+1.9$ V are shown Figs. 5(d) and (e), respectively. Fig. 5(e) reveals the same wire-like features extending along $[1\bar{1}0]$ that are observed experimentally in Fig. 5(b). The (2×7) cell is outlined by a dashed rectangle in all images. Further bias dependence is shown in Figs. 5(f) and (g) for $V_{bias} = +0.28$ V and $+0.8$ V, respectively, which is in agreement with reported experimental STM images of Dy and Gd [28] and further supports the atomic model.

From all the surface reconstruction patterns of Y/Si(001), one notes that adatoms form columns along $[1\bar{1}0]$, orthogonal to the direction of Si dimer rows. This is because RE and Y adatoms prefer to form 2- or 3-adatom chains on the hollow sites in the trench between Si dimer rows before taking sites between individual Si dimerized atoms. These adatom chains repeat to form a line along $[1\bar{1}0]$. Consequently, nanowire formation along the Si dimer row is clearly unfavorable since it would require large cooperative atomic migration. While the asymmetric strain between the hexagonal disilicide crystal structure and Si(001) explains the formation of anisotropic nanostructures, our results here provide an explanation for why nanowires are predominantly orthogonal to Si dimer rows on vicinal Si(001).

4. Conclusions

Synergistic *ab initio* calculations and STM measurements were performed in order to understand rare earth induced reconstructions on Si(001). Due to the competition between long-range Coulomb repulsion and short range hybridization, the binding energy minima correspond to configurations with 2- or 3-adatom chains. These structural models reproduced the (2×3) and (2×4) features reported in previous experimental data. Furthermore, the (2×7) reconstruction model we proposed is comprised of these two configurations. The proximity of BE values for several configurations in Fig. 1 indicates the possibility of RE monomers, dimers and trimers co-existing on Si(001), in agreement with STM observations [18,25,27,28]. The preference to form rows of Y dimers and trimers along $[1\bar{1}0]$ explains why nanowires form perpendicularly to Si dimer rows. Clearly, studies of surface reconstruction patterns are critical to understanding assembly of $RESi_2$ nanowires, essential for the optimization of their fabrication for various applications.

Acknowledgements

Acknowledgment is made to the National Science Foundation CBET-0731349. Calculations were performed on NERSC supercomputers. A.S. and R.R. acknowledge Sangyeob Lee for assisting with data acquisition.

References

[1] C. Preinesberger, S. Vandre, T. Kalka, M. Dahne-Prietsch, J. Phys. D Appl. Phys. 31 (1998) L43.
[2] B.Z. Liu, J. Nogami, Nanotechnology 14 (2003) 873.
[3] R. Ragan, Y. Chen, D.A.A. Ohlberg, G. Medeiros-Ribeiro, R.S. Williams, J. Cryst. Growth 251 (2003) 657.
[4] Y. Chen, D.A.A. Ohlberg, R.S. Williams, J. Appl. Phys. 91 (2002) 3213.
[5] R.D. Thompson, B.Y. Tsaur, K.N. Tu, Appl. Phys. Lett. 38 (1981) 535.
[6] C. Preinesberger, G. Pruskil, S.K. Becker, M. Dahne, D.V. Vyalikh, S.L. Molodtsov, C. Laubschat, F. Schiller, Appl. Phys. Lett. 87 (2005) 083107.
[7] J. Nogami, B.Z. Liu, M.V. Katkov, C. Ohbuchi, N.O. Birge, Phys. Rev. B 63 (2001) 233305.
[8] H.W. Yeom, Y.K. Kim, E.Y. Lee, K.D. Ryang, P.G. Kang, Phys. Rev. Lett. 95 (2005) 205504.
[9] K.N. Tu, R.D. Thompson, B.Y. Tsaur, Appl. Phys. Lett. 38 (1981) 626.
[10] R. Ragan, et al., Proc. SPIE 5593 (2004) 167.
[11] J.P. You, J.H. Choi, S. Kim, X.M. Li, R.S. Williams, R. Ragan, Nano Lett. 6 (2006) 1858.
[12] M. Valden, X. Lai, D.W. Goodman, Science 281 (1998) 1647.
[13] J. Grunes, J. Zhu, M.C. Yang, G.A. Somorjai, Catalysis Lett. 86 (2003) 157.
[14] A. Shinde, J. Cao, R. Wu, R. Ragan, Israel J. Chem. 48 (2008) 73.
[15] M. Kuzmin, M.P.J. Punkkinen, P. Laukkanen, R.E. Perala, M. Ahola-Tuomi, T. Balasubramanian, I.J. Vayrynen, Phys. Rev. B 78 (2008) 045318.
[16] J. Tersoff, D.R. Hamann, Phys. Rev. B 31 (1985) 805.
[17] A. Shinde, J. Cao, S. Lee, R. Wu, R. Ragan, Chem. Phys. Lett. 466 (2008) 159.
[18] A. Pratt, C. Woffinden, C. Bonet, S. Tear, Phys. Rev. B 78 (2008) 155430.
[19] B.C. Harrison, P. Ryan, J.J. Boland, Surf. Sci. 582 (2005) 79.
[20] L. Magaud, J.Y. Veuillen, D. Lollman, T.A.N. Tan, D.A. Papaconstantopoulos, M.J. Mehl, Phys. Rev. B 46 (1992) 1299.
[21] N.G. Szwacki, B.I. Yakobson, Phys. Rev. B 75 (2007) 035406.
[22] C. Rogero, C. Koitzsch, M.E. Gonzalez, P. Aebi, J. Cerda, J.A. Martin-Gago, Phys. Rev. B 69 (2004) 045312.
[23] C. Rogero, C. Polop, L. Magaud, J.L. Sacedon, P.L. de Andres, J.A. Martin-Gago, Phys. Rev. B 66 (2002) 235421.
[24] C. Ohbuchi, J. Nogami, Surf. Sci. 579 (2005) 157.
[25] J.S. Yang, Q. Cai, X.D. Wang, R. Koch, Surf. Sci. 526 (2003) 291.
[26] B.Z. Liu, J. Nogami, Surf. Sci. 488 (2001) 399.
[27] C. Ohbuchi, J. Nogami, Phys. Rev. B 66 (2002) 165323.
[28] B.Z. Liu, J. Nogami, Surf. Sci. 540 (2003) 136.
[29] Y. Chen, D.A.A. Ohlberg, G. Medeiros-Ribeiro, Y.A. Chang, R.S. Williams, Appl. Phys. Lett. 76 (2000) 4004.
[30] G. Kresse, J. Furthmuller, Phys. Rev. B 54 (1996) 11169.
[31] G. Kresse, D. Joubert, Phys. Rev. B 59 (1999) 1758.
[32] L. Martinage, J. Phys. Condens. Matter 1 (1989) 2593.
[33] S.J. Jenkins, G.P. Srivastava, J. Phys. Condens. Matter 8 (1996) 6641.